Neutron skin thickness for ^{208}Pb from total cross sections of neutron scattering at 14.137 MeV and neutron skin thickness for ^{48}Ca, O, N, C isotopes from reaction and interaction cross sections

Shingo Tagami

Department of Physics, Kyushu University, Fukuoka 819-0395, Japan

Takayuki Myo

General Education, Faculty of Engineering, Osaka Institute of Technology, Osaka 535-8585, Japan

Masanobu Yahiro*

Department of Physics, Kyushu University, Fukuoka 819-0395, Japan

Background: Foster *et al.* measured total neutron cross sections $\sigma_{\rm T}$ of n+^{208}Pb scattering at $E_{\rm lab} = 14.137$ MeV. We tested the Kyushu (chira)l g-matrix folding model for reaction cross sections $\sigma_{\rm R}$ on p+^{208}Pb scattering in $20 \lesssim E_{\rm lab} \lesssim 180$ MeV and found that our folding model is reliable. As for ^{12}C+^{12}C scattering, we tested the Kyushu g-matrix folding model and found that the folding model is reliable for $\sigma_{\rm R}$ in $30 \lesssim E_{\rm lab} \lesssim 100$ MeV/u and $250 \lesssim E_{\rm lab} \lesssim 400$ MeV/u. Ozawa *et al.* accumulated the measured values of interaction cross sections $\sigma_{\rm I}$ and the extracted matter radii $r_{\rm m}$ from ^{4}He to ^{32}Mg. Bagchi *et al.* determined proton radii $r_{\rm p}$(CC) for $^{14,15,17-22}$N by measuring the charge-changing (CC) cross sections, and found a signal of ^{22}N being a halo nucleus. Kanungo *et al.* measured the CC cross sections and extracted $r_{\rm p}$(CC) for $^{12-19}$C. Kaur *et al.* made a similar measurement and determined $r_{\rm p}$(CC) for $^{16,18-24}$O.

Purposes: Our 1st aim is to extract neutron tkin thickness $r_{\rm skin}^{208}$ from the the $\sigma_{\rm T}$ of n+^{208}Pb scattering at $E_{\rm lab} = 14.137$ MeV. Our 2nd aim is to test the Kyushu g-matrix folding model for ^{4}He+^{208}Pb scattering in $30 \lesssim E_{\rm lab} \lesssim 180$ MeV. 0ur 3rd aim is to find stable nuclei having nuclei having large $r_{\rm skin}$.

Results: We extract $r_{\rm skin}^{208} = 0.309 \pm 0.057$ fm from the $\sigma_{\rm T}$. We find that $r_{\rm skin} = 0.267 \pm 0.056$ fm for ^{14}N and $r_{\rm skin} = 0.197 \pm 0.067$ fm for ^{17}O.

Conclusion: The value $r_{\rm skin}^{208} = 0.309 \pm 0.057$ fm agrees with $r_{\rm skin}^{208}$(PREX2).

I. INTRODUCTION

Horowitz *et al.* [1] proposed a direct measurement for neutron skin thickness $r_{\rm skin} = r_{\rm n} - r_{\rm p}$, where $r_{\rm n}$ and $r_{\rm p}$ are the root-mean-square radii of neutrons and protons, respectively.

The PREX collaboration has reported [2]

$$r_{\rm skin}^{208}({\rm PREX2}) = 0.283 \pm 0.071 = 0.212\text{–}0.354\,{\rm fm}. \quad (1)$$

The CREX group has presented [3]

$$r_{\rm skin}^{48}({\rm CREX}) = 0.121 \pm 0.026\,({\rm exp}) \pm 0.024\,({\rm model})\,{\rm fm}. (2)$$

The PREX2 and CREX values are reliable for ^{208}Pb and ^{48}Ca, respectively. Using the $r_{\rm p}$ deduced from the electron scattering of Refs. [4, 5], one can obtain $r_{\rm n}$ and matter radii $r_{\rm m}$ for PREX2 and CREX, as shown in Table I.

TABLE I. Values of $r_{\rm m}$(exp), $r_{\rm n}$(exp), $r_{\rm skin}$(exp) together with $r_{\rm p}$(exp) deduced from the electron scattering [4, 5]. The radii are shown in units of fm.

.	$r_{\rm p}$(exp)	$r_{\rm m}$(exp)	$r_{\rm n}$(exp)	$r_{\rm skin}$(exp)
PREX2	5.444	5.617 ± 0.044	5.727 ± 0.071	0.283 ± 0.071
CREX	3.385	3.456 ± 0.030	3.506 ± 0.050	0.121 ± 0.050

In Ref. [6], we extracted $r_{\rm skin}^{208} = 0.278 \pm 0.035$ fm from reaction cross sections $\sigma_{\rm R}$ on p+^{208}Pb scattering, using the

chiral (Kyushu) g-matrix folding model [7, 8] with the densities calculated with Gogny-D1S HFB (D1S-GHFB) with angular momentum projection (AMP). The central value almost agrees with that of $r_{\rm skin}^{208}$(PREX2). In this paper, we try to find nucleus having thick skin-value in order to support $r_{\rm skin}^{208}$(PREX2).

In Ref. [9], we tested the Kyushu g-matrix folding model for $\sigma_{\rm R}$ on p+^{208}Pb scattering in $20 \lesssim E_{\rm lab} \lesssim 180$ MeV and find that our folding model is reliable there, using the $\sigma_{\rm R}$(PREX2) calculated with the folding model with the neutron density scaled to $r_{\rm n}^{208}$(PREX2); note that the $r_{\rm p}^{208}$ calculated with D1S-GHFB+AMP agrees with the $r_{\rm p}^{208}$(PREX2) of Ref. [5] In the paper, we extracted $r_{\rm skin}$ and $r_{\rm m}$ from the data $\sigma_{\rm R}$ for ^{208}Pb, ^{58}Ni, ^{48,40}Ca , ^{12}C targets, using the Kyushu g-matrix folding model with the densities calculated with D1S-GHFB+AMP. As a way of a fine-tuning factor f, we proposed the ESP-f (experimental scaling procedure). The ESP-f is a reliable way for ^{208}Pb, ^{58}Ni, ^{40,48}Ca, ^{12}C. As for ^{12}C, the ESP-f is nothing but a method from interaction cross sections $r_{\rm m}(\sigma_{\rm I})$ to $r_{\rm m}(\sigma_{\rm R})$.

As for ^{4}He scattering, we determined $r_{\rm skin}^{208} = 0.416 \pm 0.146$ fm for ^{208}Pb in $30 \lesssim E_{\rm lab} \lesssim 50$ MeV/u with the Kyushu g-matrix folding model with the D1S-GHFB+AMP proton and neutron densities, and extracted $r_{\rm skin}$ and $r_{\rm m}$ for ^{40}Ca and Sn isotopes [10]. In this paper, we test the Kyushu g-matrix folding model for $\sigma_{\rm R}$ on ^{4}He+^{208}Pb scattering in $30 \lesssim E_{\rm lab} \lesssim 180$ MeV with the D1S-GHFB+AMP proton and neutron densities, using the ESP-f, that is, we extracted $r_{\rm skin}^{208}$ as the $\sigma_{\rm R}$(PREX2) as a reference (reliable) value.

Foster *et al.* measured total neutron cross sections $\sigma_{\rm T}$ of

* orion093g@gmail.com

n+^{208}Pb scattering at $E_{\rm lab} = 14.137$ MeV [11]. Our aim is to extract $r_{\rm skin}^{208}$ from the the $\sigma_{\rm T}$

The measured values of $\sigma_{\rm I}$ and the extracted matter radii $r_{\rm m}(\sigma_{\rm I})$ are accumulated from ^{4}He to ^{32}Mg in Ref. [12]; see Table 1 of Ref. [12] for the $\sigma_{\rm I}$ and see Table 3 (Glauber model in the optical limit) for the $r_{\rm m}(\sigma_{\rm I})$.

Bagchi *et al.* measured charge-changing (CC) cross sections around 900 MeV/u at GSI and determined the proton radii $r_{\rm p}$(CC) for $^{14,15,17-22}$N [13]. As for ^{14,15}N, the $r_{\rm p}(e^-)$ are obtainable with the isotope shift based on electron scattering [4]. As for $A = 14, 15$, the $r_{\rm p}$(CC) are consistent with those of electron scattering. They extracted matter radii $r_{\rm m}$ and neutron skin thickness $r_{\rm skin}$ from interaction cross sections $\sigma_{\rm I}$ [12] for $^{14,15,17-22}$N, using the Glauber model where the $r_{\rm p}$(CC) were used and the neutron radius $r_{\rm n}$ were evaluated with the harmonic oscillator density. They mentioned that an increase in $r_{\rm m}$ from ^{21}N to ^{22}N is a signal of ^{22}N being a halo nucleus.

Kaur *et al.* measured charge-changing (CC) cross sections and $\sigma_{\rm I}$ for $^{16,18-24}$O+^{12}C scattering at around $900A$ MeV and presented the values of the $r_{\rm p}$(CC) and the $r_{\rm m}$ for $^{16,18-24}$O, using the Glauber model [14]; see Table I of Ref. [14]. As for $A = 16, 18$, the $r_{\rm p}$(CC) are consistent with the $r_{\rm p}(e^-)$. They also extracted $r_{\rm skin}$ from the $r_{\rm p}$(CC) and the $r_{\rm m}$ for $^{16,18-24}$O.

Kanungo *et al.* measured the CC cross sections for $^{12,14-19}$C+^{12}C scattering to determine the $r_{\rm p}$(CC) [15]. Their values are consistent with those of electron scattering for $A = 12, 14$.

Dobrovolsky *et al.* measured the absolute differential cross sections for small-angle elastic scattering of on $^{12,14-17}$C on a proton target at energies near 700 MeV/u and determined $r_{\rm m}$ for $^{12,14-17}$C by using the Glauber model. [16]. Using $r_{\rm p}(e^-)$ for ^{12,14}C and the $r_{\rm p}$(CC) of Ref. [15] for ^{15,16,17}C, they extracted $r_{\rm skin}$; see Table 2 of Ref. [16].

Reaction cross sections $\sigma_{\rm R}$, interaction cross sections $\sigma_{\rm I}$ for charged projectiles and $\sigma_{\rm I}$ for neutron are standard observable of determining $r_{\rm skin}$, when the $r_{\rm p}$(exp) is calculated with the isotope shift method based on the electron scattering [4]. Good data on $\sigma_{\rm R}$ for p+^{48}Ca scattering are available in Ref. [17].

As for ^{12}C+^{12}C scattering, we tested the Kyushu g-matrix folding model and found that the folding model [7] is reliable for $\sigma_{\rm R}$ in $30 \lesssim E_{\rm lab} \lesssim 100$ MeV and $250 \lesssim E_{\rm lab} \lesssim 400$ MeV [18].

Tanaka *et al* measured interaction cross sections $\sigma_{\rm I}$ for $^{42-51}$Ca + ^{12}C scattering at 280 MeV/nucleon and determined $r_{\rm skin}$ for $^{42-51}$Ca [19]. As for ^{48}Ca, Tanaka *et al.* extracted $r_{\rm skin}^{48} = 0.146 \pm 0.06$ fm, using the Glauber model (the optical limit) with the Woods-Saxon proton and neutron densities.

In Ref. [20], we reanalyzed the data, using the Kyushu g-matrix folding model with the D1S-GHFB densities for ^{43,45,47,49,51}Ca and the D1S-GHFB+AMP densities for ^{42,44,46,48,50}Ca. Their skin values almost agree with ours, except for ^{48}Ca. D1S is thus reliable for $^{42-47,49-51}$Ca. There is non-negligible difference between our value $r_{\rm skin}^{48} = 0.105 \pm 0.06$ fm and theirs $r_{\rm skin}^{48} = 0.146 \pm 0.06$ fm. The fact indicates that we carefully choose proton and neutron densities in order to construct proton and neutron densities for ^{48}Ca.

Only as for ^{48}Ca, we then choose D1M [21] in stead of D1S, since the D1M-GHFB+AMP calculation yields better agreement with the total energy than the D1S-GHFB+AMP one [22]. The further reason why we take D1M is shown in Sec. III C 1.

We determined $r_{\rm m}(\sigma_{\rm R})$ for ^{12}C, as shown in Table II. Our result $r_{\rm m}(\sigma_{\rm R})$ of Ref. [9] based on p+ ^{12}C scattering almost agree with that of Ref. [23] based on ^{12}C+^{12}C scattering each other. Note that there is no fine-tuning factor for ^{12}C+^{12}C scattering and we used the ESP-f for p+^{12}C scattering.

TABLE II. Values of $r_{\rm m}(\sigma_{\rm R})$ and $r_{\rm m}(\sigma_{\rm I})$. The two values $r_{\rm m}(\sigma_{\rm I})$ are taken from the accumulation paper of Ref. [12]. The first $r_{\rm m}(\sigma_{\rm R})$ are determined from the $\sigma_{\rm R}$ of p scattering in Ref. [9], whereas the 2nd $r_{\rm m}(\sigma_{\rm R})$ is extracted from the $\sigma_{\rm R}$ of ^{12}C+^{12}C scattering in Ref. [23]. The radii are shown in units of fm.

	$r_{\rm m}(\sigma_{\rm R})$	$r_{\rm m}(\sigma_{\rm R})$	$r_{\rm m}(\sigma_{\rm I})$	$r_{\rm m}(\sigma_{\rm I})$
^{12}C	2.340 ± 0.009	2.352 ± 0.013	2.31 ± 0.02	2.35 ± 0.02

The chiral nucleon-nucleon (NN) forces used in the Kyushu g-matrix folding model has a cutoff of 550 MeV. For this reason, the model is applicable for $E_{\rm lab} \lesssim 410$ MeV. At $E_{\rm lab} \gtrsim 500$ MeV, in fact, we extracted $r_{\rm skin}$ and $r_{\rm m}$ for ^{208}Pb by using the folding model [24] based on the Love-Franey (LF) t-matrix [25] model. Our $r_{\rm skin}$ values, 0.325 ± 0.076 fm for D1S+AMP and 0.333 ± 0.076 fm for D1M+AMP, are consistent with $r_{\rm skin}^{208}$(PREX2). Note that the former value is very close to the latter.

Our first aim is to extract $r_{\rm skin}^{208}$ from the the $\sigma_{\rm T}$ of Ref. [11] of n+^{208}Pb scattering at $E_{\rm lab} = 14.137$ MeV. Our 2nd aim is to test the Kyushu g-matrix folding model for ^{4}He+^{208}Pb scattering in $30 \lesssim E_{\rm lab} \lesssim 180$ MeV with $\sigma_{\rm R}$(PREX2). 0ur 3rd aim is to find stable nuclei having nuclei having large $r_{\rm skin}$.

Our model is formulated in Sec. II, and our results is shown in Sec. III. Section V is devoted to a summary.

II. MEHOD

The g-matrix folding model [7, 26–34] is a standard way of determining $r_{\rm skin}$ and/or $r_{\rm m}$ from $\sigma_{\rm R}$ and $\sigma_{\rm I}$. In the model, the potential is obtained by folding the g-matrix with projectile and target densities.

Applying the folding model based on the Melbourne g-matrix [27] for $\sigma_{\rm R}$ of Mg isotopes, we deduced the $r_{\rm m}$ for Mg isotopes [32], and discovered that ^{31}Ne is a halo nucleus with large deformation [29].

Kohno calculated the g matrix for the symmetric nuclear matter, using the Brueckner-Hartree-Fock method with chiral N^{3}LO 2NFs and NNLO 3NFs [35]. He set $c_D = -2.5$ and $c_E = 0.25$ so that the energy per nucleon can become minimum at $\rho = \rho_0$ [7].

Toyokawa *et al.* localized the non-local chiral g matrix into three-range Gaussian forms by using the localization method proposed by the Melbourne group [27, 36, 37]. The resulting local g matrix is called "Kyushu g-matrix".

The Kyushu g-matrix folding model is successful in reproducing the differential cross sections $d\sigma/d\Omega$ and the vector

analyzing power A_y for polarized proton scattering on various targets at $E_{\text{lab}} = 65$ MeV [33], and $d\sigma/d\Omega$ for ^{4}He scattering at $E_{\text{lab}} = 72$ MeV per nucleon [34]. This is true for σ_{R} of ^{4}He scattering in $E_{\text{lab}} = 30 \sim 200$ MeV per nucleon [7].

In this paper, we use the Kyushu g-matrix folding model [7] for lower energies and the LF folding model for higher energies.

In the the Kyushu g-matrix folding model, the potential U consists of the direct part (U^{DR}) and the exchange part (U^{EX}) defined by

$$U^{\text{DR}}(\boldsymbol{R}) = \sum_{\mu,\nu} \int \rho_{\text{P}}^{\mu}(\boldsymbol{r}_{\text{P}})\rho_{\text{T}}^{\nu}(\boldsymbol{r}_{\text{T}})g_{\mu\nu}^{\text{DR}}(s)d\boldsymbol{r}_{\text{P}}d\boldsymbol{r}_{\text{T}}, \quad (3)$$

$$U^{\text{EX}}(\boldsymbol{R}) = \sum_{\mu,\nu} \int \rho_{\text{P}}^{\mu}(\boldsymbol{r}_{\text{P}}, \boldsymbol{r}_{\text{P}} - \boldsymbol{s})\rho_{\text{T}}^{\nu}(\boldsymbol{r}_{\text{T}}, \boldsymbol{r}_{\text{T}} + \boldsymbol{s})$$
$$\times g_{\mu\nu}^{\text{EX}}(s) \exp\left[-i\boldsymbol{K}(\boldsymbol{R}) \cdot \boldsymbol{s}/M\right]d\boldsymbol{r}_{\text{P}}d\boldsymbol{r}_{\text{T}}, \quad (4)$$

where $\boldsymbol{s} = \boldsymbol{r}_{\text{P}} - \boldsymbol{r}_{\text{T}} + \boldsymbol{R}$ for the coordinate $\boldsymbol{R}$ between a projectile (P) and a target (T). The coordinate $\boldsymbol{r}_{\text{P}}$ ($\boldsymbol{r}_{\text{T}}$) denotes the location for the interacting nucleon measured from the center-of-mass of P (T) and $M = AA_{\text{T}}/(A + A_{\text{T}})$ for the mass number A (A_{T}) of P (T). Each of μ and ν stands for the z-component of isospin; 1/2 means neutron and $-1/2$ does proton.

The direct and exchange parts, $g_{\mu\nu}^{\text{DR}}$ and $g_{\mu\nu}^{\text{EX}}$, of the g matrix are described by

$$g_{\mu\nu}^{\text{DR}}(s) = \frac{1}{4}\sum_{S} \hat{S}^2 g_{\mu\nu}^{S1}(s) \text{ for } \mu + \nu = \pm 1, \quad (5)$$

$$g_{\mu\nu}^{\text{DR}}(s) = \frac{1}{8}\sum_{S,T} \hat{S}^2 g_{\mu\nu}^{ST}(s) \text{ for } \mu + \nu = 0, \quad (6)$$

$$g_{\mu\nu}^{\text{EX}}(s) = \frac{1}{4}\sum_{S} (-1)^{S+1}\hat{S}^2 g_{\mu\nu}^{S1}(s) \text{ for } \mu + \nu = \pm 1, \quad (7)$$

$$g_{\mu\nu}^{\text{EX}}(s) = \frac{1}{8}\sum_{S,T} (-1)^{S+T}\hat{S}^2 g_{\mu\nu}^{ST}(s) \text{ for } \mu + \nu = 0, \quad (8)$$

where $\hat{S} = \sqrt{2S+1}$ and $g_{\mu\nu}^{ST}$ are the spin-isospin components of the g-matrix interaction. The Kyushu g-matrix [7] is constructed from the chiral 2NFs and 3NFs interaction with the cutoff 550 MeV. In the LF t-matrix folding model, the chiral g-matrix is placed by the LF t-matrix. [25] The formulation for proton+nucleus scattering is shown in Ref. [31].

As for a ^{12}C target, we use the phenomenological density of Ref. [38]. We use the Gogny-D1S Hartree-Fock-Bogoliubov (D1S-GHFB) method for O-isotope densities, since effects of angular momentum projection (AMP) are negligible for spherical nuclei such as O isotopes. As C isotopes, we use the D1S+GHFB+AMP densities for $A = 14, 16, 18$ and the phenomenological one for $A = 12$. As odd nuclei such as N isotopes, the D1S+GHFB+AMP method is not feasible; this point is explained in Ref. [18]. We use SLy7 [10, 39, 40] that is an improved version of SLy4. The SLy7 were used for ^{4}He+^{208}Pb scattering in order to extract $r_{\text{skin}}^{208} = 0.416 \pm 0.146$ fm [10]. As for ^{208}Pb, the SLy7 yields the same r_{m} as D1S-GHFB+AMP. This is true for N isotopes.

The scaled density $\rho_{\text{scaling}}(\boldsymbol{r})$ is obtained from the original projectile density $\rho(\boldsymbol{r})$ as

$$\rho_{\text{scaling}}(\boldsymbol{r}) = \frac{1}{\alpha^3}\rho(\boldsymbol{r}/\alpha) \quad (9)$$

with a scaling factor

$$\alpha = \sqrt{\frac{\langle \boldsymbol{r}^2 \rangle_{\text{scaling}}}{\langle \boldsymbol{r}^2 \rangle}}. \quad (10)$$

In order to extract the r_{m} from the measured σ_{I} and σ_{R}, we scale the proton and neutron densities so as to reproduce the σ_{I} under the condition that $r_{\text{p,scaling}} = r_{\text{p}}(\text{exp})$, where $r_{\text{p}}(\text{exp})$ stands for either $r_{\text{p}}(\text{e}^-)$ or $r_{\text{p}}(\text{CC})$; note that $Ar_{\text{m}}^2 = Zr_{\text{p}}^2 + Nr_{\text{n}}^2$.

A. Relation between the Kyushu t-matrix folding model and the LF t-matrix folding model

Now, we compare the LF t-matrix folding model with the Kyushu t-matrix folding model for ^{12}C+^{12}C scattering at $30 \lesssim E_{\text{lab}} \lesssim 950$ MeV/u. The difference between the results of the Kyushu g-matrix folding model and those of the Kyushu t-matrix folding model is small at $E_{\text{lab}} = 372$ MeV. Since the chiral t-matrix has a cutoff of 550 MeV, the results of the chiral t-matrix folding model are reliable in $E_{\text{lab}} \lesssim 410$ MeV/u, where we use the phenomenological projectile and target densities for both the models. The results of the Kyushu t-matrix folding model agree with those of the LF t-matrix folding model $F\sigma_R^{\text{LF}}$ with $F = 0.93766$ at $E_{\text{lab}} = 410$ MeV/u.

As shown in Fig. 1, the fine-tuning factor F satisfies $\sigma_{\text{I}}(\text{exp}) = F\sigma_{\text{R}}(\text{LF})$ for ^{12}C+^{12}C scattering at 790 and 950 MeV/nucleon, as shown in Fig. 1. In $350 \lesssim E_{\text{lab}} \lesssim 400$ MeV/nucleon, the results of Kyushu t-matrix folding model almost agree with $F\sigma_R^{\text{LF}}$ with $F = 0.93766$, where σ_R^{LF} is the σ_R calculated with the LF t-matrix folding model.

The F is used for scattering of C, N, O isotopes on a ^{12}C target.

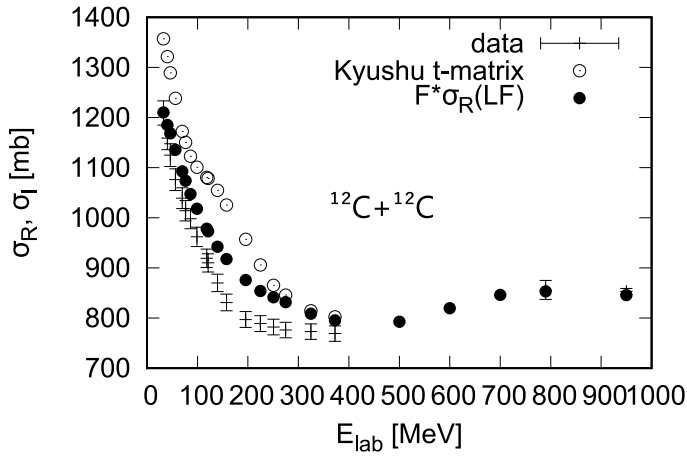FIG. 1. E_{lab} dependence of σ_{R} and σ_{I} for ^{12}C+^{12}C scattering. Open circles stand for the results of the Kyushu t-matrix folding model with the phenomenological projectile and target densities. Closed circles correspond to the $F\sigma_{\text{R}}(\text{LF})$ with $F = 0.93766$. The data are taken from Refs. [12, 41–43].

III. RESULTS

A. Determination of r_{skin}^{208} from the the total cross sections at $E_{\text{lab}} = 14.137$ MeV

Figure 2 shows E_{lab} dependence of σ_{T} for n+^{208}Pb scattering. Closed circles denote the the total cross sections $\sigma_{\text{T}}(\text{PREX2})$ calculated with the folding model with the neutron density scaled to $r_{\text{n}}^{208}(\text{PREX2})$, where the r_{p}^{208} calculated with D1S-GHFB+AMP agrees with the $r_{\text{p}}^{208}(\text{PREX2})$ of Ref. [5]
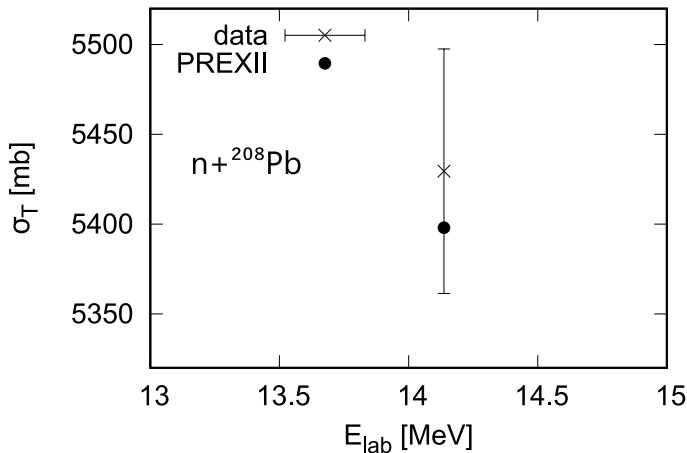

FIG. 2. E_{lab} dependence of σ_{T} for n+^{208}Pb scattering at $E_{\text{lab}} = 14.137$ MeV. Closed circles denote the the total cross sections $\sigma_{\text{T}}(\text{PREX2})$ calculated with the folding model with the neutron density scaled to $r_{\text{n}}^{208}(\text{PREX2})$, where the r_{p}^{208} calculated with D1S-GHFB+AMP agrees with the $r_{\text{p}}^{208}(\text{PREX2})$ of Ref. [5] The data are taken from Ref. [11].

Scaling the neutron PREX2 density for ^{208}Pb with the ESP-f method to the data [11] on the total cross sections at 14.137 MeV, we can obtain $r_{\text{skin}}^{208} = 0.309 \pm 0.057$ fm. The value agrees with $r_{\text{skin}}^{208}(\text{PREX2})$.

Figure 3 shows total cross sections σ_{T} of n+^{208}Pb scattering as a function of E_{lab}. An open circle stands for the result of the Woods-Saxon type neutron density ($r_{WS} = 6.59$ fm, $a_{WS} = 0.7$ fm) fitted to the central value of PREX2 and the D1S-GHFB+AMP neutron density, and a close circle denotes the result of the Woods-Saxon type neutron density ($r_{WS} = 6.81$ fm, $a_{WS} = 0.6$ fm) and the D1S-GHFB+AMP neutron density. The former (latter) result is near the upper (lower) bound of the data [11]. The central value of the data [11] indicates $a_{WS} \approx 0.65$ fm.
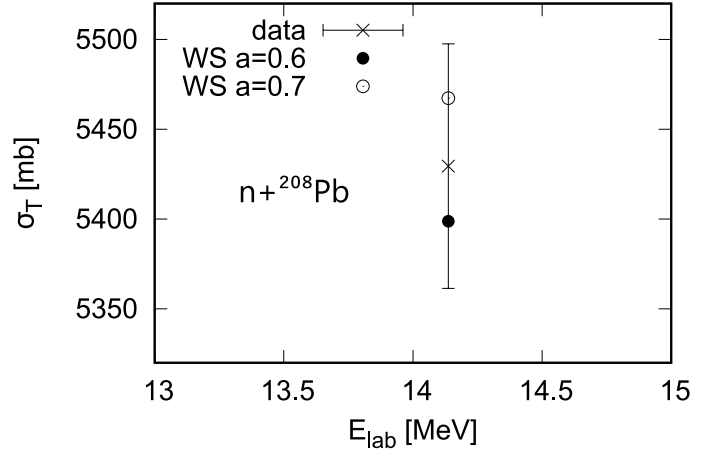

FIG. 3. E_{lab} dependence of σ_{T} for n+^{208}Pb scattering at $E_{\text{lab}} = 14.137$ MeV. An open circle stands for the result of the Woods-Saxon type neutron density ($r_{WS} = 6.59$ fm, $a_{WS} = 0.7$ fm) fitted to the central value of PREX2 and the D1S-GHFB+AMP proton density, and a close circle denotes the result of the Woods-Saxon type neutron density($r_{WS} = 6.81$ fm, $a_{WS} = 0.6$ fm) and the D1S-GHFB+AMP proton density. The data are taken from Ref. [11].

B. Test of the Kyushu g-matrix folding model for ^{4}He+^{208}Pb scattering in $30 \lesssim E_{\text{lab}} \lesssim 180$ MeV

Figure 4 shows E_{lab} dependence of σ_{R} for ^{4}He+^{208}Pb scattering. Closed circles denote the $\sigma_{\text{R}}(\text{PREX2})$ calculated with the folding model with the neutron density scaled to $r_{\text{n}}^{208}(\text{PREX2})$, where the r_{p}^{208} calculated with D1S-GHFB+AMP agrees with the $r_{\text{p}}^{208}(\text{PREX2})$ of Ref. [5]

The $\sigma_{\text{R}}(\text{PREX2})$ reproduce the data [44, 45] at 29.3, 40.975, 48.1 MeV/u. In our previous paper [10], the data at 29.3, 40.975, 48.1 MeV/u yield $r_{\text{skin}}^{208} = 0.416 \pm 0.146$ fm. Nevertheless, the value is larger than $r_{\text{skin}}^{208}(\text{PREX2})$. The central values of the data should decrease as E_{lab} tends to zero in the energy range of $E_{\text{lab}} \lesssim 41$ Mev because of the Coulomb barrier, since $\sigma_{\text{R}}(\text{PREX2})$ has such a E_{lab} dependence. However, the data at at 29.3 MeV/u is larger than that that at 40.975 MeV/u. We should neglect the data at 29.3 MeV/u.

Scaling the neutron PREX2 density with the ESP-f method to the data at 40.975, 48.1 MeV/u, we obtain $r_{\rm skin}^{208} = 0.241 \pm 0.304$ fm that is consistent with $r_{\rm skin}^{208}({\rm PREX2})$.
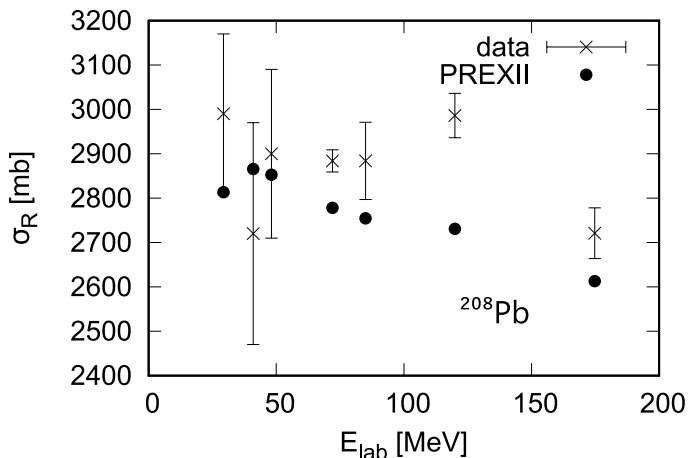

FIG. 4. $E_{\rm lab}$ dependence of $\sigma_{\rm R}$ for $^4{\rm He}+^{208}{\rm Pb}$ scattering in $30 \lesssim E_{\rm lab} \lesssim 180$ MeV. Closed circles denote the $\sigma_{\rm R}({\rm PREX2})$ calculated with the folding model with the neutron density scaled to $r_{\rm n}^{208}({\rm PREX2})$, where the $r_{\rm p}^{208}$ calculated with D1S-GHFB+AMP agrees with the $r_{\rm p}^{208}({\rm PREX2})$ of Ref. [5] The data are taken from Refs. [44, 45].

As for ^{4}He, the gaussian expansion method (GEM) [46] as ab initio calculations is applied for ^{4}He in which the Argonne V8' NN interaction (AV8) and the phenomenological three-nucleon interaction are used [47]. The NNN interaction is adjusted so as to reproduce the binding energies of ^{4}He. As for ^{4}He, the matter density of the ground state is shown in Fig. 2 of Ref. [47].

Using the GEM proton and neutron densities for ^{4}He, we obtain $r_{\rm skin}^{208} = 0.264 \pm 0.303$ fm. The central value is very close to that $r_{\rm skin}^{208}({\rm PREX2})$.

C. Reanalyses for ^{48}Ca

1. Comparison between D1S and D1M for ^{48}Ca

Figure 5 shows $\sigma_{\rm R}$ as a function of $E_{\rm lab}$ for $p+^{48}$Ca scattering. The results of the D1M-GHFB+AMP densities yield better agreement with the data [17] than those of the D1S-GHFB+AMP densities. This is true for $^{48}{\rm Ca}+^{12}$C scattering at 280 MeV/nuleon [19], as shown in Fig. 6.
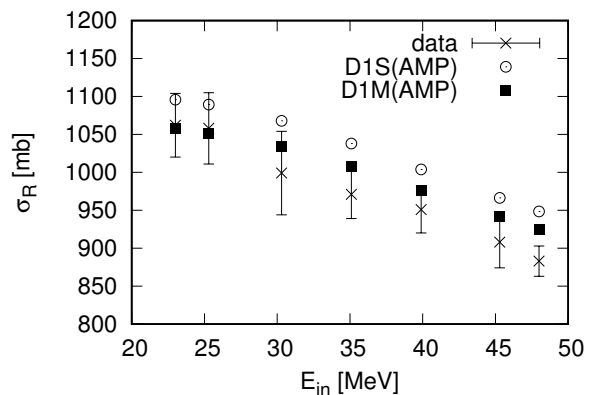

FIG. 5. $E_{\rm lab} = E_{\rm in}$ dependence of reaction cross sections $\sigma_{\rm R}$ for $p+^{48}$Ca scattering in $E_{\rm lab} = 23$–48 MeV. Circles denote results of the D1S-GHFB+AMP densities, and squares correspond to those of the D1M-GHFB+AMP densities The data (crosses) are taken from Ref. [17].

FIG. 6. Interaction cross sections $\sigma_{\rm I}$ for $^{48}{\rm Ca}+^{12}$C scattering at 280 MeV/nucleon. Circles denote results of the D1S-GHFB+AMP densities, and squares correspond to those of the D1M-GHFB+AMP densities The data (crosses) are taken from Ref. [19].
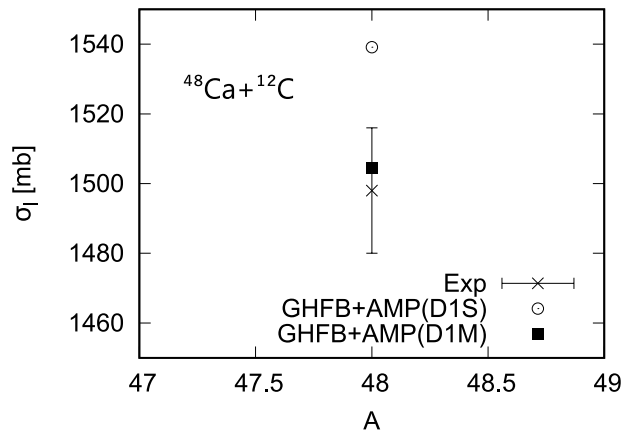
D1M is thus better than D1S for both $p+^{48}$Ca and $^{48}{\rm Ca}+^{12}$C scattering.

2. $^{48}Ca+^{12}C$ scattering in $E_{lab} = 280$ MeV/u

Figure 6 shows $\sigma_{\rm I}$ for $^{48}{\rm Ca}+^{12}$C scattering at 280 MeV/nucleon. Scaling the D1M-GHFB+AMP proton and neutron densities for ^{48}Ca , we can obtain

$$r_{\rm skin}^{48}({\rm skin}) = 0.180 \pm 0.058 \text{ fm}. \qquad (11)$$

Since we do not adopt any fine-tuning factor, we use the re-sulting values of Table III as reference values for ^{48}Ca. We can obtain $r_{\rm m}({\rm CREX})$ and $r_{\rm n}({\rm CREX})$ from the CREX value

of Eq. (2) and $r_p(\text{exp}) = 3.385$ fm [4] of electron scattering. Our value on $r_m(\text{exp})$ is slightly larger than those of CREX. As shown in Table III, the r_n of D1M-GHFB+AMP is very close to the result $r_n(\text{ref})$ determined from $^{48}\text{Ca}+^{12}\text{C}$ scattering.

TABLE III. Values of $r_m(\text{exp})$, $r_n(\text{exp})$, $r_{\text{skin}}(\text{exp})$ together with $r_p(\text{exp})$ deduced from the electron scattering [4]. The radii are shown in units of fm.

Ref.	$r_p(\text{exp})$	$r_m(\text{exp})$	$r_n(\text{exp})$	$r_{\text{skin}}(\text{exp})$
^{48}Ca CREX	3.385	3.456 ± 0.030	3.506 ± 0.050	0.121 ± 0.050
^{48}Ca ref	3.385	3.491 ± 0.035	3.565 ± 0.058	0.180 ± 0.058
^{48}Ca D1M	3.417	3.504	3.564	0.147

3. $p+^{48}Ca$ scattering in $E_{\text{lab}} = 23$–48 MeV

The $\sigma_R(\text{ref})$ calculated with the Kyushu g-matrix folding model with the proton and neutron densities having $r_p(\text{ref})$ and $r_n(\text{ref})$ are compared with the data [17] in Fig. 7. The fine-tuning factor f is obtained by averaging $\sigma_R(\text{exp})/\sigma_R(\text{ref})$ over E_{lab}. The resulting value is $f = 0.968537$. The $f \sigma_R(\text{ref})$ are scaled so as to reproduce the data [17]. This procedure is nothing but ESP-F.
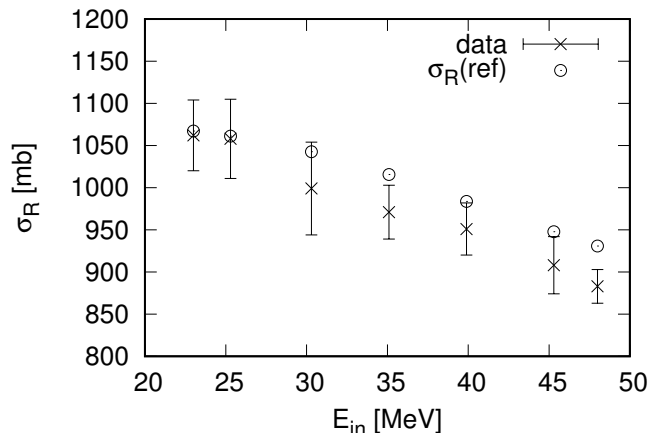

FIG. 7. Reaction cross sections σ_R as a function of $E_{\text{lab}} = E_{\text{in}}$ for $p+^{48}\text{Ca}$ scattering in $E_{\text{lab}} = 23$–48 MeV. Open circles denote results of $\sigma_R(\text{ref})$. The data (crosses) are taken from Ref. [17].

The resulting skin value is

$$r^{48}_{\text{skin}}(\text{skin}) = 0.163 \pm 0.037 \text{ fm.} \tag{12}$$

The results are tabulated in Table IV. Our skin value is consistent with $r^{48}_{\text{skin}}(\text{CREX})$, as shown in Table IV.

TABLE IV. Values of $r_m(\text{exp})$, $r_n(\text{exp})$, $r_{\text{skin}}(\text{exp})$ together with $r_p(\text{exp})$ deduced from the electron scattering [4]. The radii are shown in units of fm.

Ref.	$r_p(\text{exp})$	$r_m(\text{exp})$	$r_n(\text{exp})$	$r_{\text{skin}}(\text{exp})$
^{48}Ca CREX	3.385	3.456 ± 0.030	3.506 ± 0.050	0.121 ± 0.050
^{48}Ca TW	3.385	3.481 ± 0.022	3.548 ± 0.037	0.163 ± 0.037

D. Analyses of σ_I

Our $r_m(\sigma_I)$ values calculated with the LF t-matrix folding model are consistent with those in Table 3 (optical limit) of Ref. [12] for N, O, C isotopes. As for N isotopes, our $r_m(\sigma_I)$, however, agree with the upper bound of $r_m(\sigma_I)$ of Ref. [13] for $A = 14, 15, 17$–22. The consistency between our skin values $r_{\text{skin}}(\sigma_I)$ and those of previous works [13–15] are shown blow.

1. N isotopes

We use the data σ_I [12, 42, 48, 49] for $^{14-23}\text{N}+^{12}\text{C}$ scattering in 710–1020 MeV/u; see Table 1 of Ref. [12] for the values of σ_I.

Figure 8 shows A dependence of interaction cross sections σ_I for $^{14-23}\text{N}+^{12}\text{C}$ scattering, where A is the mass number. The LF t-matrix folding model overshoots σ_I [12, 42, 48, 49]. The renormalized $F\sigma_R(\text{LF})$ with $F = 0.93766$ reproduces the data [12, 42, 48, 49].
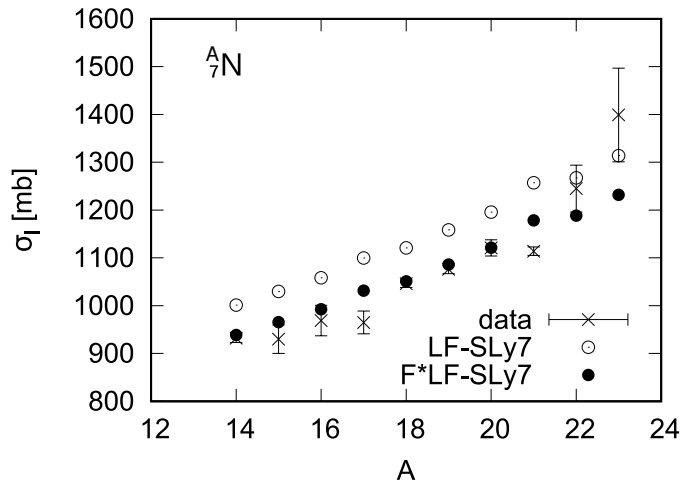

FIG. 8. A dependence of interaction cross sections σ_I for $^A\text{N}+^{12}\text{C}$ scattering. Open circles stand for the results of the LF t-matrix folding model with the SLy7 densities. Closed circles correspond to those of $F\sigma_R(\text{LF})$. The data are taken from Refs. [12, 42, 48, 49]; see Table 1 of Ref. [12].

The SLy7 proton and neutron densities are scaled so that

the $F\sigma_R(LF)$ can reproduce the data under the condition of $r_{p,scaling} = r_p(exp)$.

Our results thus obtained are tabulated in Table V. The $r_{skin}(\sigma_I)$ of ^{14}N is close to PREX2 value.

TABLE V. Values on r_p, r_m, r_n, r_{skin} for N isotopes. The r_p are deduced from the charge radii [4] for $^{14,15}N$ and the $r_p(CC)$ of Ref. [13] are used for $A = 17$–22.

A	r_{skin}	error	r_m	error	r_n	error	r_p	error
14	0.259	0.079	2.553	0.042	2.680	0.079	2.42041	0.000
15	0.091	0.175	2.523	0.096	2.565	0.175	2.47402	0.000
17	0.010	0.182	2.556	0.079	2.560	0.152	2.55	0.03
18	0.368	0.106	2.761	0.038	2.898	0.076	2.53	0.03
19	0.432	0.105	2.801	0.041	2.952	0.075	2.52	0.03
20	0.531	0.128	2.876	0.059	3.051	0.098	2.52	0.03
21	0.565	0.099	2.879	0.040	3.055	0.069	2.49	0.03
22	0.828	0.212	3.119	0.127	3.358	0.182	2.53	0.03
16			2.608	0.227				
23			3.415	0.220				

Figure 11 shows A dependence of the r_{skin} for $^{14,15,17-22}N$. Our skin values are compared with those of Ref. [13]. Our results are slightly larger than theirs.
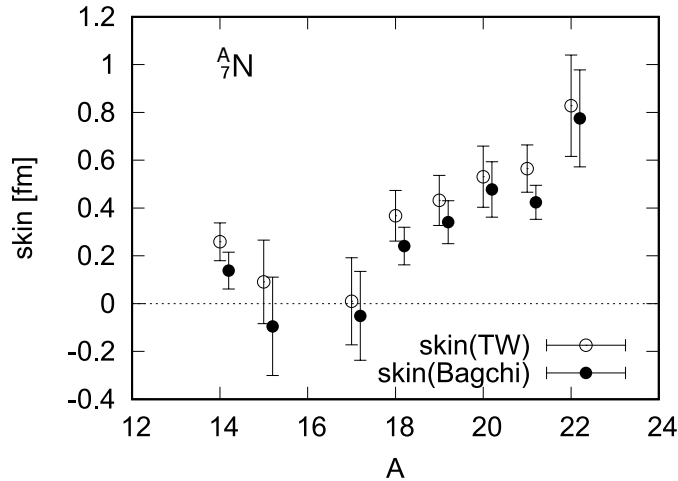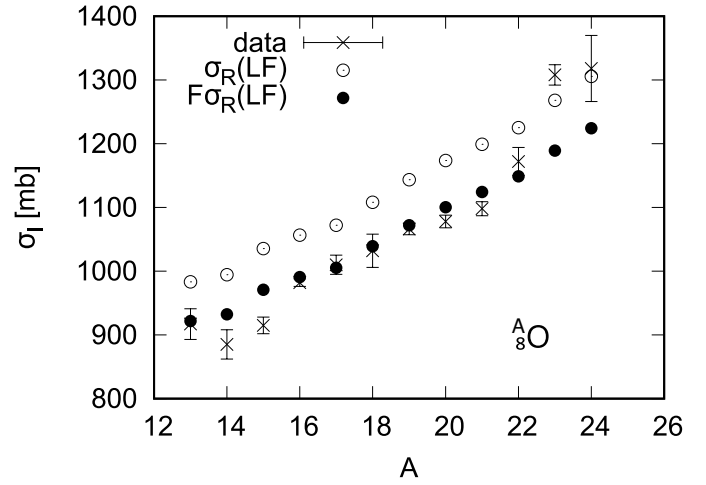

FIG. 9. Comparison between our results and those of Ref. [13] for r_{skin} for $^{14,15,17-22}N$.

2. O isotopes

The same procedure is taken for O isotopes. As shown in Fig. 10, the LF t-matrix folding model overshoots the data σ_I of Refs. [12, 42, 50] in $A = 13$–22. The $F\sigma_R(LF)$ with $F = 0.93766$ reproduce the data in $A = 13$–22.

FIG. 10. A dependence of interaction cross sections σ_I for $^A O + ^{12}C$ scattering. Open circles stand for the results of the LF t-matrix folding model with the D1S-GHFB proton and neutron densities in the spherical limit. Closed circles correspond to those of $F\sigma_R(LF)$. The data are taken from Table 1 of Ref. [12].

The D1S-HFB proton and neutron densities in the spherical limit are scaled so that the $F\sigma_R(LF)$ can reproduce the data under the condition of $r_{p,scaling} = r_p(exp)$.

Our results for O isotopes are tabulated in Table VI. The skin value is larger for ^{17}O.

TABLE VI. Values on r_p, r_m, r_n, r_{skin} for O isotopes. The r_p are based on the charge radii [4] for $^{16,17,18}O$ and the $r_p(CC)$ of Ref. [14] for $A = 19$–24.

A	r_{skin}	error	r_m	error	r_n	error	r_p	error
16	0.027	0.030	2.582	0.015	2.596	0.030	2.569	0.000
17	0.197	0.067	2.672	0.037	2.763	0.067	2.566	0.000
18	0.059	0.111	2.684	0.063	2.710	0.111	2.651	0.000
19	0.322	0.088	2.741	0.024	2.872	0.058	2.55	0.03
20	0.409	0.072	2.783	0.026	2.939	0.052	2.53	0.02
21	0.380	0.070	2.771	0.026	2.910	0.050	2.53	0.02
22	0.633	0.101	2.919	0.049	3.133	0.081	2.50	0.02
23	0.895	0.089	3.192	0.034	3.475	0.059	2.58	0.03
24	0.975	0.202	3.193	0.108	3.485	0.162	2.51	0.04
13			2.532	0.063				
14			2.401	0.061				
15			2.420	0.034				

As for O isotopes, our r_{skin} values are slightly larger than those of Ref. [14] for $A = 16, 18$–24. As for $A = 13$–24, as shown in Fig. 11.
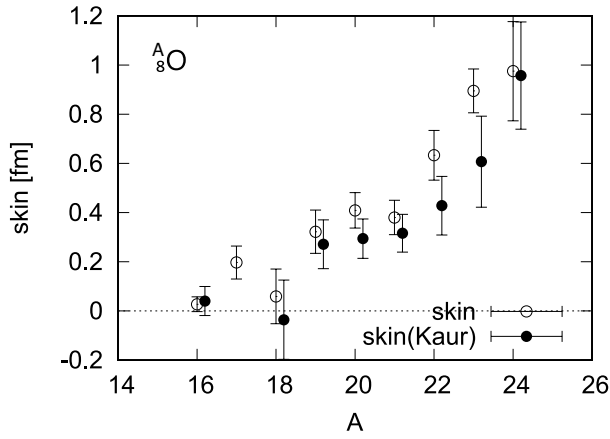
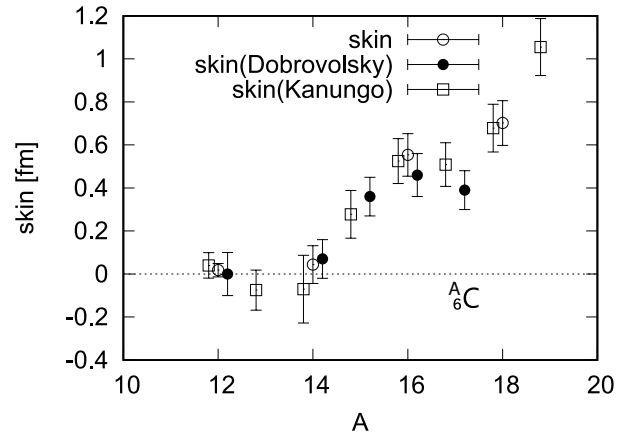FIG. 11. Comparison of $r_{\rm skin}$ between ours and those of Ref. [14] for O isotopes.

FIG. 12. Comparison of $r_{\rm skin}$ between ours and those of Refs. [15, 16] for C isotopes.

3. C isotopes

As for ^{12}C+^{12}C scattering, the $F\sigma_{\rm R}$(LF) reproduces the data [12, 41] at 790, 950 MeV/u within error-bars, as shown in Fig. 1. The phenomenological proton and neutron densities are scaled so as to reproduce the data under the condition of $r_{\rm p,scaling} = r_{\rm p}({\rm exp})$. The average of two $r_{\rm m}$ values is taken.

The projectile ^{12}C densities should be the same as the target ^{12}C ones. The reason why we use the phenomenological densities are that the $r_{\rm m}({\rm th})$ of the phenomenological matter densities yield better agreement with the experimental values of Table II than that of the D1S-GHFB+AMP matter densities

The same procedure is taken for ^{14,16,18}C+^{12}C scattering in which the D1S-GHFB+AMP proton and neutron densities for ^{14,16,18}C.

Our results for C isotopes are tabulated in Table VII.

TABLE VII. Values on $r_{\rm p}$, $r_{\rm m}$, $r_{\rm n}$, $r_{\rm skin}$ for C isotopes. The $r_{\rm p}$ are deduced from the charge radii [4] for ^{12,14}C and $r_{\rm p}$(CC) of Ref. [15] are used for $A = 16, 18$.

A	$r_{\rm skin}$	error	$r_{\rm m}$	error	$r_{\rm n}$	error	$r_{\rm p}$	error
12	0.058	0.031	2.356	0.016	2.385	0.031	2.327	0.000
14	0.079	0.087	2.415	0.051	2.449	0.088	2.370	0.000
16	0.586	0.099	2.781	0.027	2.986	0.059	2.400	0.040
18	0.733	0.104	2.900	0.035	3.123	0.064	2.390	0.040

Figure 12 shows A dependence of $r_{\rm skin}$ for $^{12-18}$C. Our $r_{\rm skin}$ values are consistent with those of Refs. [15, 16].

4. Shell effects

We analyzed the data $\sigma_{\rm I}$ [20] on $^{42-51}$Ca+^{12}C scattering by using Kyushu (chiral) g-folding model with D1S-GHFB proton and neutron densities with and without AMP.

Figure 13 shows our $r_{\rm n}$ of Ref. [20] values as a function of N for $^{42-51}$Ca. Our $r_{\rm n}$ values are minimized at $N = 28$. This is the fact that $N = 28$ is a major shell.
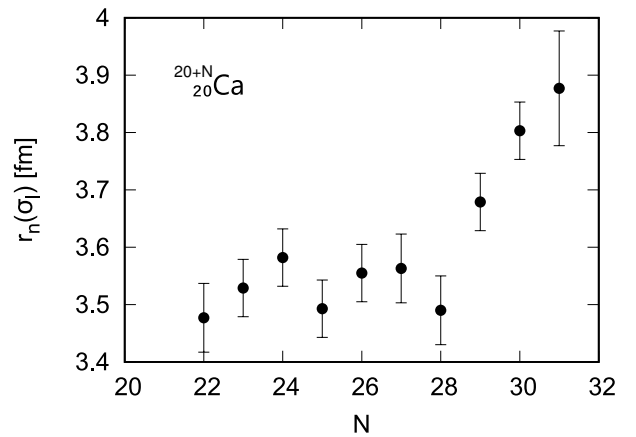

FIG. 13. N dependence of $r_{\rm n}$ for $^{42-51}$Ca.

Figure 14 shows our $r_0(N) = r_{\rm m}(N)/A^{1/3}$ values as a function of N for $^{42-51}$Ca. Our $r_0(N)$ values also have a dip in $N = 28$. The $r_0(N)$ are useful to find a major shell.
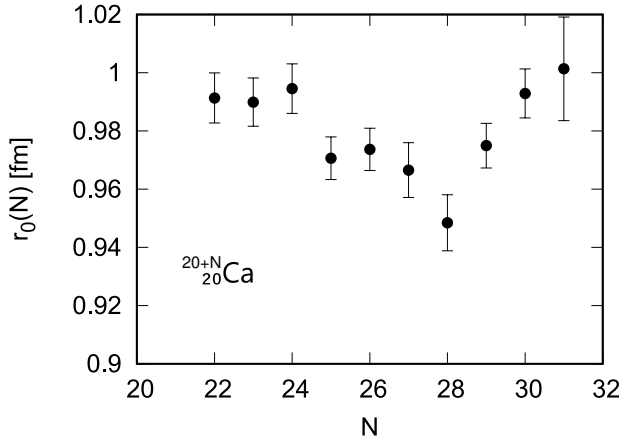
FIG. 14. N dependence of $r_0(N) = r_{\mathrm{m}}(N)/A^{1/3}$ for $^{42-51}$Ca.

Now, we consider the case of O, N, C isotopes by using $r_0(N)$.

Figure 15 shows N dependence of $r_0(N) = r_{\mathrm{m}}(N)/A^{1/3}$ for O,N, C isotopes. The $r_0(N)$ are minimized at $N = 14$ for N isotopes, This indicates the fact that $N = 14$ is a sub-shell. The $r_0(N)$ are minimized at $N = 8$ for N, C isotopes. This shows the fact that $N = 8$ is a major-shell,
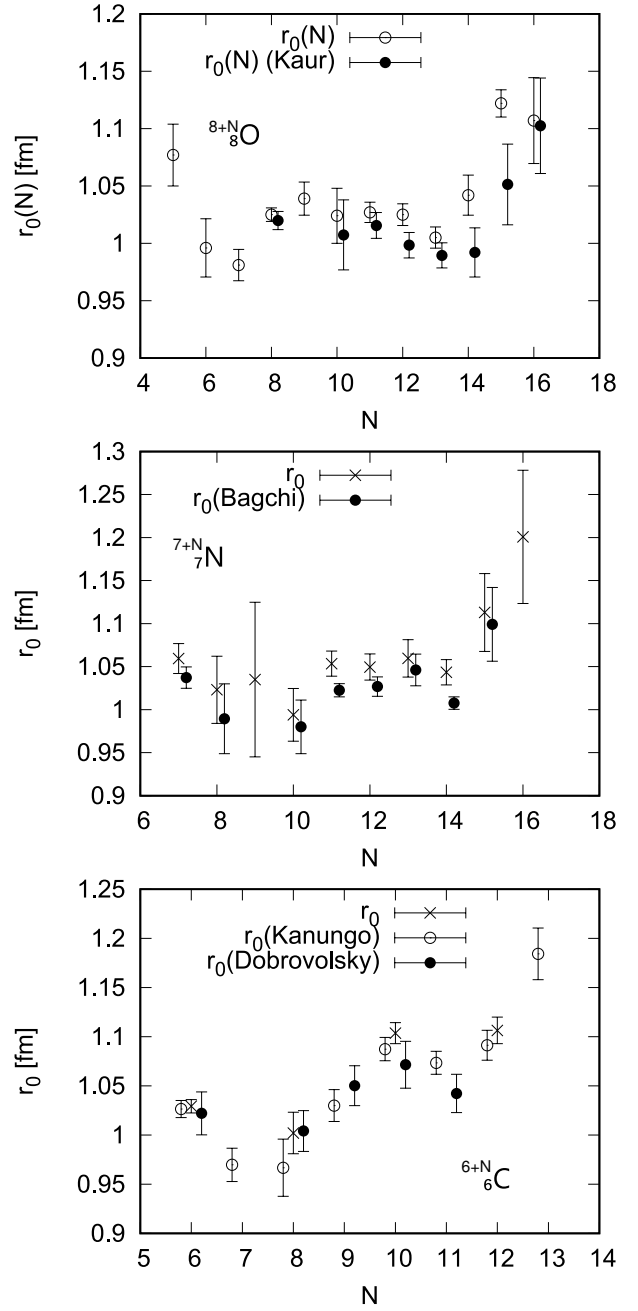

FIG. 15. Comparison of $r_0(N) = r_{\mathrm{m}}(N)/A^{1/3}$ between ours and those of Ref. [14] for O isotopes, of Ref. [13] for N isotopes, of Refs. [15, 16] for C isotopes.

5. Relation between r_{m} and total binding energy for N isotopes

As for N isotopes, the data on $\beta \equiv r_{\mathrm{m}}E_{\mathrm{B}}/(A\hbar c)$ hardly depend on A for $A = 14$–22; note that E_{B}/A is the binding energy per nucleon. In fact, the deviation of β is much smaller than the average value; namely,

$$\beta = 0.0977(6) \tag{13}$$

for $A = 14$–22. This indicates that r_m is inversely proportion to E_B/A.

E. Analyses of σ_R based on p scattering

Our $r_\mathrm{m}(\sigma_\mathrm{R})$ and $r_\mathrm{skin}(\sigma_\mathrm{R})$ calculated with the Kyushu g-matrix folding model are shown blow. As for N isotopes, the $r_\mathrm{m}(\mathrm{th})$ calculated with SLy7 agree with those with D1S-GHFB within 0.2 %.

1. p+^{14}N scattering

We extract $r_\mathrm{m}(\sigma_\mathrm{R})$ from the data [51] $\sigma_\mathrm{R}(\mathrm{exp})$ for p+^{14}N scattering, using the Kyushu g-matrix folding model with the Sly7 proton and neutron densities.

Figure 16 shows our values on σ_R and the data [51]. The Kyushu g-matrix folding model with the SLy7 densities almost agrees with the data [51]. We then introduce a fine-tuning factor f. We use the ESP-f of Ref. [9] in order to determine f. The fine-tuning factor f is obtained by averaging $\sigma_\mathrm{R}(\mathrm{exp})/\sigma_\mathrm{R}(\mathrm{th})$ over E_lab. The resulting value is $f = 0.86196$. we obtain $r_\mathrm{m}(\sigma_\mathrm{R})$, as shown in Table VIII. The $r_\mathrm{m}(\sigma_\mathrm{R})$ is larger than $r_\mathrm{m}(\sigma_\mathrm{I})$ shown in Table VIII. The $r_\mathrm{skin}(\sigma_\mathrm{R})$ of ^{14}N is even close to PREX2 value.
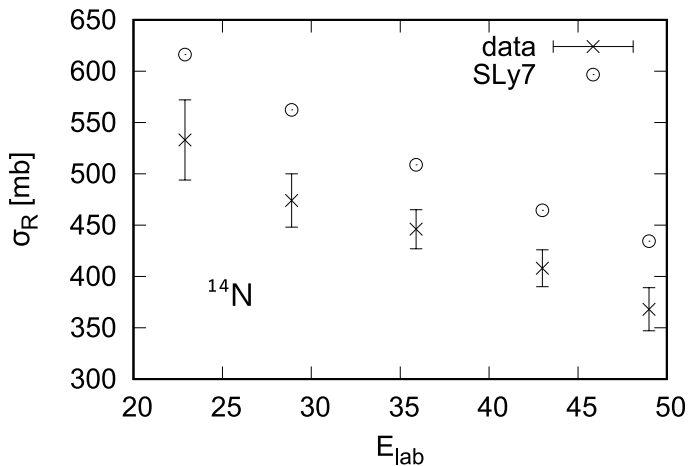

FIG. 16. E_lab dependence of σ_R for p+^{14}N scattering. Open circles stand for results of the Kyushu g-matrix folding model with the SLy7 densities. The data is taken from Refs. [51].

TABLE VIII. Values on $r_\mathrm{m}(\sigma_\mathrm{R})$, r_p,r_n, r_skin for ^{14}N based on proton scattering.

A	$r_\mathrm{skin}(\sigma_\mathrm{R})$	error	$r_\mathrm{m}(\sigma_\mathrm{R})$	error	r_n	error	r_p
14	0.267	0.056	2.558	0.029	2.688	0.056	2.42041

2. p+^{16}O scattering

In Ref. [52], the σ_R have been measured for ^{12}C, ^{16}O targets at 65.5 MeV. We first derive $\sigma_\mathrm{R}(\mathrm{th})$ with the Kyushu g-matrix folding model with the phenomenological proton and neutron densities of ^{12}C and introduce a fine-tuning factor f as $f = \sigma_\mathrm{R}(\mathrm{exp})/\sigma_\mathrm{R}(\mathrm{th}) = 0.92449$. The reason why we take the phenomenological proton and neutron densities is that the phenomenological matter radius $r_\mathrm{m}(\sigma_\mathrm{ph})$ of ^{12}O, ^{16}O are close to the corresponding experimental values, as shown in Table II and Table IX. Applying the f value to p+^{16}O scattering at 65.5 MeV and scaling the the phenomenological densities of ^{16}O, we obtain $r_\mathrm{m}(\sigma_\mathrm{R}) = 2.584 \pm 0.053$ fm for ^{16}O. The value is consistent with $r_\mathrm{m}(\sigma_\mathrm{I})$, as shown in Table IX.

TABLE IX. Values of $r_\mathrm{m}(\sigma_\mathrm{R})$ and $r_\mathrm{m}(\sigma_\mathrm{I})$. The values $r_\mathrm{m}(\sigma_\mathrm{I})$ are taken from Ref. [12]. The radii are shown in units of fm.

	$r_\mathrm{m}(\sigma_\mathrm{R})$	$r_\mathrm{m}(\sigma_\mathrm{ph})$	$r_\mathrm{m}(\sigma_\mathrm{I})$
^{12}C		2.3375	
^{16}O	2.584 ± 0.053	2.5914	2.54 ± 0.02

F. Halo nature

Tanihata *et al.* determined r_m for $^{6-9,11}$Li, ^{12}C from σ_I at 790 MeV/u [41] and found that ^{11}Li is a halo nucleus; see Refs. [12, 41] for the r_m.

We extracted r_skin for ^{6,8}He by using the LF t-matrix folding model. The nature of halo is defined only qualitatively. Meanwhile, r_skin is defined quantitatively: For halo nuclei, the r_skin are 0.778 ± 0.041 fm for ^{6}He, 0.975 ± 0.204 fm ^{11}Li [4, 12, 41], 0.853 ± 0.071 fm for ^{11}Be [4, 12, 42]; see Ref. [53] for the derivation. In Fig. 8 of Ref. [54], we showed A dependence of r_skin for Ne isotopes, where A is the mass number. The $r_\mathrm{skin} \approx 0.52$ fm for ^{31}Ne is much larger than those of ^{30,32}Ne. These large skin values come from the halo nature. This makes it possible to define the halo nature with r_skin. However, for ^{22}C as a heaviest halo nucleus at the present stage, we cannot extract r_skin, since r_p is unknown.

As for ^{22}C, a large increase in the σ_R of ^{22}C+p scattering from that of ^{20}C+p scattering [55] was observed. Here ^{21}C is unbound. Adding p to ^{21}C yields ^{22}N that is a weakly-bound nucleus having the single-neutron separation energy $s_\mathrm{n} = 1.54$ MeV. This implies that ^{22}N is a halo nucleus described by the ^{21}N+n two-body model. The increase of σ_R or σ_I is thus important. For the case of ^{22}N, we then define the nature of halo quantitatively as

$$\mathcal{H}_1 = \frac{4\pi r_\mathrm{m}(^{22}\mathrm{N})^2 - 4\pi r_\mathrm{m}(^{21}\mathrm{N})^2}{4\pi r_\mathrm{m}(^{22}\mathrm{N})^2} \qquad (14)$$

and

$$\mathcal{H}_2 = \frac{s_\mathrm{n}(^{22}\mathrm{N})}{E_\mathrm{B}(^{22}\mathrm{N})/A} \qquad (15)$$

The nature of halo is realized, when $\mathcal{H}_1$ are large and $\mathcal{H}_2$ is small. Our results of Table V yield $\mathcal{H}_1 = 0.148$ and $\mathcal{H}_2 = 0.241$ for ^{22}N. For ^{22}C with $s_{2n} = 10$ keV [12, 55], we get $\mathcal{H}_1 = 0.695$ and $\mathcal{H}_2 = 0.001$. For ^{11}Li with $s_{2n} = 0.369$ MeV [41], we obtain $\mathcal{H}_1 = 0.447$ and $\mathcal{H}_2 = 0.044$. We consider that ^{22}N is halo-like.

1. Deformation for ^{12,14,16,18}C

In Ref. [56], Li, Luo and Wang compiled the charge radii Rch of 236 nuclei measured by laser spectroscopy experiment, and calculated the uncertainties. From the Rch of Mg isotope chain, the new magic number $N = 14$ can be observed. They introduced Eq. (5) for Rch. However, C, N, O isotopes are not included in the 236 nuclei.

Using Eq. (5) of Ref. [56], we took the shell corrections (SC) for ^{16,24}O, since the SC are shown in Ref. [57]. Using the parameter set (Table A) of Ref. [56], we show A dependence of Rch$(WS - 1)$, Rch$(HFB25 - 1)$, Rch$(WS - 1 + SC)$, where the Rch$(WS - 1 + SC)$ include SC but the Rch$(WS - 1)$ and the Rch$(HFB25 - 1)$ do not.

In Fig. 17, for simplicity, we take the deformation parameters $\beta_2 = 0$ and $\beta_4 = 0$. As for ^{16,17,18}O, the Rch are taken from Ref. [4]. As for $^{19--24}$O, the proton radii of Ref. [14] are transformed into the corresponding Rch. The data [4, 14] on Rch are compared with the Rch$(WS - 1)$, the Rch$(HFB25 - 1)$, the Rch$(WS - 1 + SC)$. As for ^{16,24}O, the Rch$(WS - 1 + SC)$ are larger than the data. When $\beta_2 > 0$, the Rch$(WS - 1 + SC)$ increase. This fact indicates that one should not use Eq. (5) of Ref. [56].
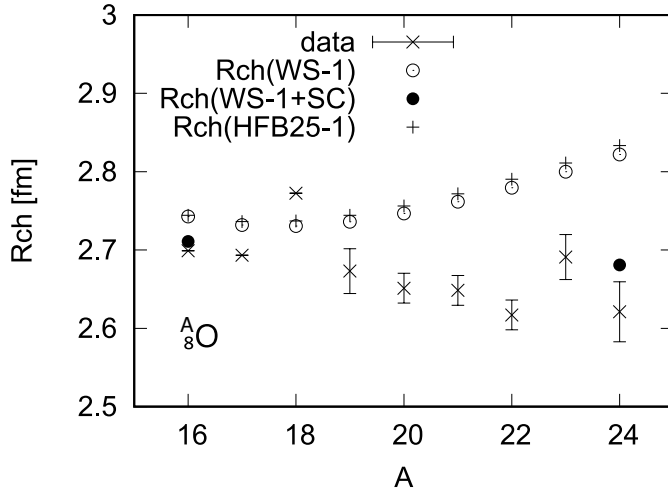

FIG. 17. A dependence of Rch$(WS - 1)$, Rch$(HFB25 - 1)$. Open circles denote the Rch$(WS - 1)$, whereas the symbol "+" corresponds to the Rch$(HFB25 - 1)$. Closed circles stand for Rch$(WS - 1 + SC)$. The data (crosses) are taken from Refs. [4, 14].

SLy7 and D1S show that N, O isotopes are spherical. We then consider deformation on C isotopes. D1S-GHFB+AMP

yields $\beta_2 = $ -0.378, -0.211, -0.307, -0.345 for ^{12,14,16,18}C, respectively. There is the famous equation on deformation:

$$r_\mathrm{m}^2 = r_\mathrm{m,0}^2 \lfloor 1 + \frac{5\beta_2^2}{4\pi} \rfloor, \tag{16}$$

where $r_\mathrm{m,0}$ is the matter radius in the spherical limit. Using the equation, we can extract $r_\mathrm{m,0}$ from r_m.

Figure shows $r_\mathrm{m,0}$ and the data (Table VII) on r_m for ^{12,14,16,18}C. Deformation effects for the r_m are about 14.8% for ^{12,14,16,18}C.
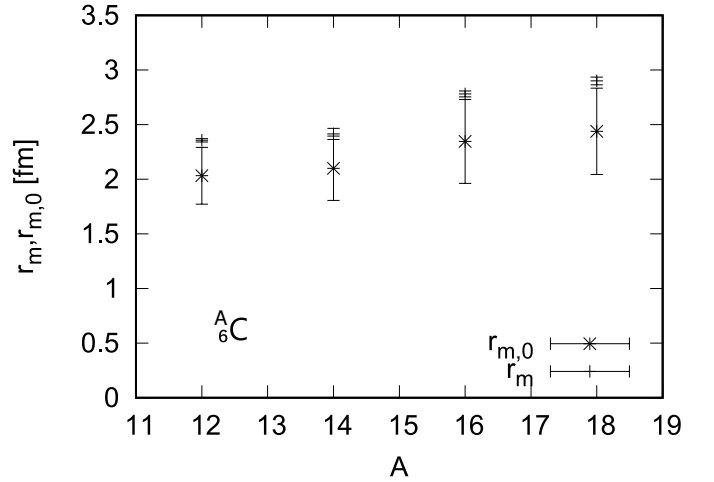

FIG. 18. A dependence of r_m, $r_\mathrm{m,0}$. The $r_\mathrm{m,0}$ have errorbars with "*", whereas the r_m correspond to errorbars with "-".

2. D1S and SLy7 for $r$skin on N isotopes

The $r_\mathrm{skin}(SLy7)$ calculated with SLy7 are compared with the $r_\mathrm{skin}(D1S)$ with D1S in Fig. 19. The $r_\mathrm{skin}(SLy7)$ are almost the same as $r_\mathrm{skin}(D1S)$ except for for ^{21}N. The difference between $r_\mathrm{skin}(SLy7)$ and $r_\mathrm{skin}(D1S)$ is appreciable only for ^{21}N. In fact, the $r_\mathrm{skin}(D1S)$ is 0.443 ± 0.221 fm, whereas $r_\mathrm{skin}(SLy7) = 0.565 \pm 0.099$ fm. As for ^{208}Pb, the difference is very small [10].

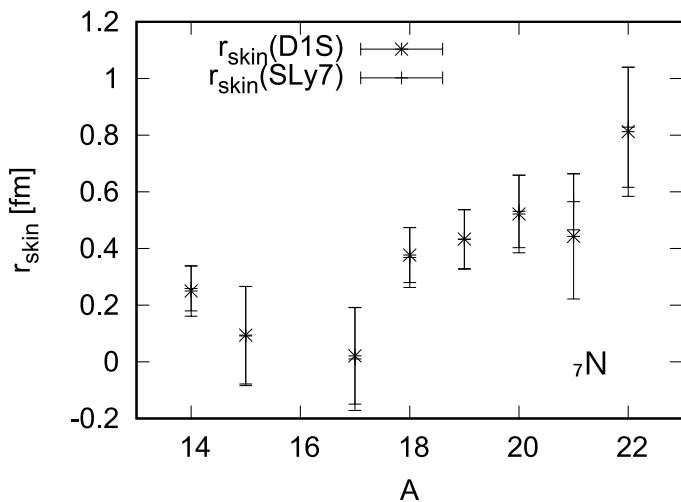FIG. 19. A dependence of $r_{\mathrm{skin}}(\mathrm{SLy7})$, $r_{\mathrm{skin}}(\mathrm{D1S})$. The $r_{\mathrm{skin}}(\mathrm{D1S})$ have errorbars with ''*'', whereas the $r\mathrm{m}$ correspond to errorbars with ''-''.

IV. DISCUSSIONS FOR MODEL DEPENDENCE

We use the Kyushu g-matrix folding model with no fine-tuning factor ($F = 1$) in $E_{\mathrm{lab}} \lesssim 410$ MeV/u and the LF t-matrix folding model with the fine-tuning F in $E_{\mathrm{lab}} \gtrsim 410$ MeV/u. The model dependence stems from (A) the proton and neutron densities used and (B) F. In Sec. III, our errors only come from those of $\sigma_{\mathrm{T}}^{\mathrm{exp}}$ and $\sigma_{\mathrm{R}}^{\mathrm{exp}}$. We can minimize the errors based on (A) by choosing the EoS yielding that the proton and neutron scaling factor being close to 1. In general, D1S and SLy7(SLy4) are good. As for ^{48}, D1M is better than D1S, as shown in Sec. III C 3. The errors based on (B) are investigated below.

As for ^{12}C+^{12}C scattering at $30 \lesssim E_{\mathrm{lab}} \lesssim 950$ MeV/u, the σ_{R} of the Kyushu t-matrix folding model agree with those of the LF t-matrix folding model $F\sigma_R^{\mathrm{LF}}$ with $F = 0.93766$ at $E_{\mathrm{lab}} = 410$ MeV/u, as shown in Fig. 1. We then used the $F = 0.93766$ value for C, N, O isotopes. As an another fitting, we may use $\sigma_{\mathrm{R}}^{\mathrm{exp}} = F\sigma_R^{\mathrm{LF}}$ at 790 MeV/u. The value is $F = 0.94096 = 0.93766 \times 1.0035$. In order to investigate influence of F, we increase the $F = 0.93766$ value by 0.35%. As for O isotopes, the central values of r_{m} decrease by 0.33%.

Now we consider coupled-channel effects in the present folding model. In $E_{\mathrm{lab}} \lesssim 410$ MeV/u, we use chiral (Kyushu) g-matrix folding model with no fine-tuning factor. The chiral g-matrix include approximately coupled-channel effects as nuclear-medium effects obtained by solving the Brueckner-Hartree-Fock method, since the chiral g-matrix include the back-coupling from all the continuum states; see Ref. [7] for the detained explanation.

Now we consider compound nucleus effects. Compound nucleus effects appear at low incident energies and are a result of multiple NN collisions. The effects decrease as E_{lab} increases from 2.491 MeV to 14.137 MeV in Ref. [11]; note that the compound -nucleus outgoing processes appear only in s-wave. We then take $E_{\mathrm{lab}} = 14.137$ MeV as an incident neutron-beam energy generated from Li(d,n). In fact, the central value of $\sigma_{\mathrm{T}}(\mathrm{PREX2})$ is very close to that of the $\sigma_{\mathrm{T}}(\mathrm{exp})$ [11], as shown in Fig. 2. The small difference between our present value $r_{\mathrm{skin}}^{208} = 0.309 \pm 0.057$ fm and $r_{\mathrm{skin}}^{208}(\mathrm{PREX2})$ may come from compound nucleus effects.

V. SUMMARY

Foster *et al.* made high-precision measurement for total neutron cross sections σ_{T} [11] of n+^{208}Pb scattering at $E_{\mathrm{lab}} = 14.137$ MeV. We extract $r_{\mathrm{skin}}^{208} = 0.309 \pm 0.057$ fm from the σ_{T}, using the chiral (Kyushu) g-matrix folding model with the D1S-GHFB+AMP proton and neutron densities. The value agrees with $r_{\mathrm{skin}}^{208}(\mathrm{PREX2})$ and is consistent with $r_{\mathrm{skin}}^{208} = 0.278 \pm 0.035$ fm [6] from σ_{R} on p+^{208}Pb scattering.

As for ^{48}Ca, we determine $r_{\mathrm{skin}}^{48}(\mathrm{skin}) = 0.163 \pm 0.037$ fm from the σ_{R} [17] on p+^{48}Ca scattering, using the Kyushu g-matrix folding model with the D1M-GHFB+AMP proton and neutron densities. We show that D1M-GHFB+AMP is better than D1S-GHFB+AMP for the matter radius and the binding energy. Our skin value is consistent with $r_{\mathrm{skin}}^{48}(\mathrm{CREX})$.

As for ^{4}He, the Gaussian expansion method (GEM) [46] as ab initio calculations is applied for ^{4}He [47]. Using the Kyushu g-matrix folding model with the D1S-GHFB+AMP proton and neutron densities for ^{208}Pb and the GEM proton and neutron densities for ^{4}He, we obtain $r_{\mathrm{skin}}^{208} = 0.264 \pm 0.303$ fm from σ_{R} of ^{4}He+^{208}Pb scattering at 40.975, 48.1 MeV/u. The value is very close to that $r_{\mathrm{skin}}^{208}(\mathrm{PREX2})$.

Using the Kyushu g-matrix and the LF folding model, among O, N, C isotopes, we find that $r_{\mathrm{skin}} = 0.267 \pm 0.056$ fm for ^{14}N and $r_{\mathrm{skin}} = 0.197 \pm 0.067$ fm for ^{17}O as stable nuclei having large skin value. The value $r_{\mathrm{skin}} = 0.267 \pm 0.056$ fm for ^{14}N is consistent with $r_{\mathrm{skin}}^{208}(\mathrm{PREX2})$. The value $r_{\mathrm{skin}} = 0.197 \pm 0.067$ fm for ^{17}O is close to $r_{\mathrm{skin}}^{208}(\mathrm{PREX2})$.

As for the nucleus having the property $Z = N$, the r_{skin} is zero, if the Coulomb interaction is switched off in the Hamiltonian for ^{14}N. This is because the realistic NN interaction is invariant under the interchange between proton and neutron. The thick skin value shows that the Coulomb effects are important.

The $r_0(N) = r_{\mathrm{m}}(N)/A^{1/3}$ are useful to find a major and a sub-major shell. When the $N = 8$ core is hard, there should be no dip. In fact, there is no dip for O isotopes. As for N, C isotopes, there appears a dip at $N = 8$, indicating that the $N = 8$ core becomes soft. As for O, N, C isotopes, there appears a dip at $N = 14$, indicating that the $N = 14$ core is a soft one.

[1] C. J. Horowitz, S. J. Pollock, P. A. Souder, and R. Michaels, Parity violating measurements of neutron densities, Phys. Rev. C **63**, 025501 (2001).

[2] D. Adhikari et al. (PREX), Accurate Determination of the Neutron Skin Thickness of ^{208}Pb through Parity-Violation in Electron Scattering, Phys. Rev. Lett. **126**, 172502 (2021), arXiv:2102.10767 [nucl-ex].

[3] D. Adhikari et al. (CREX), Precision Determination of the Neutral Weak Form Factor of Ca48, Phys. Rev. Lett. **129**, 042501 (2022), arXiv:2205.11593 [nucl-ex].

[4] I. Angeli and K. P. Marinova, Table of experimental nuclear ground state charge radii: An update, Atom. Data Nucl. Data Tabl. **99**, 69 (2013).

[5] B. A. Brown, Constraints on the Skyrme Equations of State from Properties of Doubly Magic Nuclei, Phys. Rev. Lett. **111**, 232502 (2013), arXiv:1308.3664 [nucl-th].

[6] S. Tagami, T. Wakasa, J. Matsui, M. Yahiro, and M. Takechi, Neutron skin thickness of Pb208 determined from the reaction cross section for proton scattering, Phys. Rev. C **104**, 024606 (2021), arXiv:2010.02450 [nucl-th].

[7] M. Toyokawa, M. Yahiro, T. Matsumoto, and M. Kohno, Effects of chiral three-nucleon forces on ^{4}He-nucleus scattering in a wide range of incident energies, PTEP **2018**, 023D03 (2018), arXiv:1712.07033 [nucl-th].

[8] S. Tagami, M. Tanaka, M. Takechi, M. Fukuda, and M. Yahiro, Chiral g-matrix folding-model approach to reaction cross sections for scattering of ca isotopes on a c target, Phys. Rev. C **101**, 014620 (2020).

[9] T. Wakasa, S. Tagami, J. Matsui, M. Takechi, and M. Yahiro, Neutron-skin values and matter and neutron radii determined from reaction cross sections of proton scattering on C12, Ca40,48, Ni58, and Pb208, Phys. Rev. C **107**, 024608 (2023), arXiv:2211.16688 [nucl-th].

[10] M. Matsuzaki, S. Tagami, and M. Yahiro, Neutron skin thickness of Pb208, Sn116,120,124, and Ca40 determined from reaction cross sections of He4 scattering, Phys. Rev. C **104**, 054613 (2021), arXiv:2107.06441 [nucl-th].

[11] D. G. Foster and D. W. Glasgow, Neutron total cross sections, 2.5-15 mev. i. experimental, Phys. Rev. C **3**, 576 (1971).

[12] A. Ozawa, T. Suzuki, and I. Tanihata, Nuclear size and related topics, Nucl. Phys. A **693**, 32 (2001).

[13] S. Bagchi et al., Neutron skin and signature of the $N = 14$ shell gap found from measured proton radii of $^{17-22}$N, Phys. Lett. B **790**, 251 (2019), arXiv:1901.09707 [nucl-ex].

[14] S. Kaur et al., Proton distribution radii of $^{16-24}$O: signatures of new shell closures and neutron skin, Phys. Rev. Lett. **129**, 142502 (2022), arXiv:2209.00722 [nucl-ex].

[15] R. Kanungo et al., Proton Distribution Radii of $^{12-19}$C Illuminate Features of Neutron Halos, Phys. Rev. Lett. **117**, 102501 (2016), arXiv:1608.08697 [nucl-ex].

[16] A. V. Dobrovolsky et al., Nuclear matter distributions in the neutron-rich carbon isotopes $^{14-17}$C from intermediate-energy proton elastic scattering in inverse kinematics, Nucl. Phys. A **1008**, 122154 (2021), arXiv:2101.10687 [nucl-ex].

[17] R. F. Carlson, A. J. Cox, N. E. Davison, T. Eliyakut-Roshko, R. H. McCamis, and W. T. H. v. Oers, Proton total reaction cross-sections for Ca-42, Ca-44, and Ca-48 between 21 and 48 MeV, Phys. Rev. C **49**, 3090 (1994).

[18] S. Tagami, M. Tanaka, M. Takechi, M. Fukuda, and M. Yahiro, Chiral g-matrix folding-model approach to reaction cross sections for scattering of Ca isotopes on a C target, Phys. Rev. C **101**, 014620 (2020), arXiv:1911.05417 [nucl-th].

[19] M. Tanaka et al., Swelling of Doubly Magic ^{48}Ca Core in Ca Isotopes beyond $N = 28$, Phys. Rev. Lett. **124**, 102501 (2020), arXiv:1911.05262 [nucl-ex].

[20] M. Takechi, T. Wakasa, S. Tagami, J. Matsui, and M. Yahiro, Reanalyzes for 42–51ca scattering on a 12c target at 280 mev/nucleon based on chiral g folding mode with gogny-d1s hartree–fock–bogoliubov densities, Results in Physics **31**, 104923 (2021).

[21] C. Gonzalez-Boquera, M. Centelles, X. Viñas, and L. M. Robledo, New Gogny interaction suitable for astrophysical applications, Phys. Lett. B **779**, 195 (2018), arXiv:1712.06735 [nucl-th].

[22] S. Tagami, T. Wakasa, M. Takechi, J. Matsui, and M. Yahiro, Neutron skin in 48ca determined from p+48ca and 48ca+12c scattering, Results in Physics **33**, 105155 (2022).

[23] S. Tagami, T. Wakasa, and M. Yahiro, 12c+12c scattering as the reference system for reaction cross section, Results in Physics **51**, 106675 (2023).

[24] T. Wakasa, S. Tagami, and M. Yahiro, Skin values of 208pb and 48ca determined from reaction cross sections, Results in Physics **43**, 106101 (2022).

[25] W. G. Love and M. A. Franey, Phys. Rev. C **24**, 1073 (1981).

[26] F. A. . Brieva and J. Rook, Nucl. Phys. **A291**, 299 (1977).

[27] K. Amos, P. J. Dortmans, H. V. von Geramb, S. Karataglidis, and J. Raynal, Advances in Nuclear Physics, edited by J. W. Negele and E. Vogt, Vol. 25 (Plenum, New York, 2000) p. 275.

[28] T. Furumoto, Y. Sakuragi, and Y. Yamamoto, Phys. Rev. C **78**, 044610 (2008).

[29] K. Minomo, T. Sumi, M. Kimura, K. Ogata, Y. R. Shimizu, and M.Yahiro, Phys. Rev. Lett. **108**, 052503 (2012).

[30] T. Sumi, K. Minomo, S. Tagami, M. Kimura, T. Matsumoto, K. Ogata, Y. R. Shimizu, and M. Yahiro, Deformation of Ne isotopes in the island-of-inversion region, Phys. Rev. C **85**, 064613 (2012), arXiv:1201.2497 [nucl-th].

[31] K. Egashira, K. Minomo, M. Toyokawa, T. Matsumoto, and M. Yahiro, Microscopic optical potentials for ^{4}He scattering, Phys. Rev. C **89**, 064611 (2014), arXiv:1404.2735 [nucl-th].

[32] S. Watanabe et al., Ground-state properties of neutron-rich Mg isotopes, Phys. Rev. C **89**, 044610 (2014), arXiv:1404.2373 [nucl-th].

[33] M. Toyokawa, K. Minomo, M. Kohno, and M. Yahiro, Roles of chiral three-nucleon forces in nucleon–nucleus scattering, J. Phys. G **42**, 025104 (2015), [Erratum: J.Phys.G 44, 079502 (2017)], arXiv:1404.6895 [nucl-th].

[34] M. Toyokawa, M. Yahiro, T. Matsumoto, K. Minomo, K. Ogata, and M. Kohno, Microscopic calculations based on chiral two- and three-nucleon forces for proton- and ^{4}He-nucleus scattering, Phys. Rev. C **92**, 024618 (2015), [Erratum: Phys.Rev.C 96, 059905 (2017)], arXiv:1507.02807 [nucl-th].

[35] M. Kohno, Phys. Rev. C **88**, 064005 (2013).

[36] H. V. von Geramb et al., Phys. Rev. C **44**, 73 (1991).

[37] K. Amos and P. J. Dortmans, Phys. Rev. C **49**, 1309 (1994).

[38] H. de Vries, C. W. de Jager, and C. de Vries, NUCLEAR CHARGE-DENSITY-DISTRIBUTION PARAMETERS, At. Data Nucl. Data Tables **36**, 495 (1987).

[39] E. Chabanat, P. Bonche, P. Haensel, J. Meyer, and R. Schaeffer, A Skyrme parametrization from subnuclear to neutron star densities. 2. Nuclei far from stablities, Nucl. Phys. A **635**, 231 (1998), [Erratum: Nucl.Phys.A 643, 441–441 (1998)].

[40] N. Schunck et al., Solution of the Skyrme-Hartree–Fock–Bogolyubovequations in the Cartesian deformed harmonic-oscillator basis. (VIII) hfodd (v2.73y): A new version of the program, Comput. Phys. Commun. **216**, 145 (2017), arXiv:1612.05314 [nucl-th].

[41] I. Tanihata, T. Kobayashi, O. Yamakawa, S. Shimoura, K. Ekuni, K. Sugimoto, N. Takahashi, T. Shimoda, and H. Sato, Measurement of Interaction Cross-Sections Using Isotope Beams of Be and B and Isospin Dependence of the Nuclear Radii, Phys. Lett. B **206**, 592 (1988).

[42] A. Ozawa et al., Measurements of interaction cross sections for light neutron-rich nuclei at relativistic energies and determination of effective matter radii, Nucl. Phys. A **691**, 599 (2001).

[43] M. Takechi et al., Reaction cross sections at intermediate energies and Fermi-motion effect, Phys. Rev. C **79**, 061601 (2009).

[44] A. Ingemarsson, J. Nyberg, P. Renberg, O. Sundberg, R. Carlson, A. Cox, A. Auce, R. Johansson, G. Tibell, D. T. Khoa, and R. Warner, New results for reaction cross sections of intermediate energy particles on targets from 9be to 208pb, Nuclear Physics A **676**, 3 (2000).

[45] B. Bonin, N. Alamanos, B. Berthier, G. Bruge, H. Faraggi, J. Lugol, W. Mittig, L. Papineau, A. Yavin, J. Arvieux, L. Farvacque, M. Buenerd, and W. Bauhoff, Alpha-nucleus elastic scattering at intermediate energies, Nuclear Physics A **445**, 381 (1985).

[46] H. Kameyama, M. Kamimura, and Y. Fukushima, Coupled-rearrangement-channel Gaussian-basis variational method for trinucleon bound states, Phys. Rev. C **40**, 974 (1989).

[47] E. Hiyama, B. F. Gibson, and M. Kamimura, Four-body calculation of the first excited state of He-4 using a realistic nn interaction: He-4(e, e-prime) He-4(02+) and the monopole sum rule, Phys. Rev. C **70**, 031001 (2004).

[48] A. Ozawa et al., Interaction cross-sections and radii of mass number A = 17 isobars (N-17, F-17, and Ne-17), Phys. Lett. B **334**, 18 (1994).

[49] L. Chulkov et al., Interaction cross-sections and matter radii of A = 20 isobars, Nucl. Phys. A **603**, 219 (1996).

[50] A. Ozawa, I. Tanihata, T. Kobayashi, Y. Sugahara, O. Yamakawa, K. Omata, K. Sugimoto, D. Olson, W. Christie, and H. Wieman, Interaction cross sections and radii of light nuclei, Nucl. Phys. A **608**, 63 (1996).

[51] R. Carlson, A. Cox, T. Nasr, M. De Jong, D. Ginther, D. Hasell, A. Sourkes, W. van Oers, and D. Margaziotis, Measurements of proton total reaction cross sections for 6li, 7li, 14n, 20ne and 40ar between 23 and 49 mev, Nuclear Physics A **445**, 57 (1985).

[52] A. Ingemarsson, J. Nyberg, P. Renberg, O. Sundberg, R. Carlson, A. Auce, R. Johansson, G. Tibell, B. Clark, L. Kurth Kerr, and S. Hama, Reaction cross sections for 65 mev protons on targets from 9be to 208pb, Nuclear Physics A **653**, 341 (1999).

[53] The value for ^{6}He is taken from Ref. [58]. The value for ^{11}Li is calculated from $r_{\mathrm{m}} = 3.12 \pm 0.16$ fm [12, 41] and $r_{\mathrm{p}} = 2.381$ fm deduced from the charge radius [4], and the value for ^{11}Be is from $r_{\mathrm{m}} = 2.91 \pm 0.05$ fm [12, 42] and $r_{\mathrm{p}} = 2.338$ fm deduced from the charge radius [4].

[54] T. Sumi, K. Minomo, S. Tagami, M. Kimura, T. Matsumoto, K. Ogata, Y. R. Shimizu, and M. Yahiro, Deformation of ne isotopes in the region of the island of inversion, Phys. Rev. C **85**, 064613 (2012).

[55] K. Tanaka, T. Yamaguchi, T. Suzuki, T. Ohtsubo, M. Fukuda, D. Nishimura, M. Takechi, K. Ogata, A. Ozawa, T. Izumikawa, T. Aiba, N. Aoi, H. Baba, Y. Hashizume, K. Inafuku, N. Iwasa, K. Kobayashi, M. Komuro, Y. Kondo, T. Kubo, M. Kurokawa, T. Matsuyama, S. Michimasa, T. Motobayashi, T. Nakabayashi, S. Nakajima, T. Nakamura, H. Sakurai, R. Shinoda, M. Shinohara, H. Suzuki, E. Takeshita, S. Takeuchi, Y. Togano, K. Yamada, T. Yasuno, and M. Yoshitake, Observation of a large reaction cross section in the drip-line nucleus ^{22}C, Phys. Rev. Lett. **104**, 062701 (2010).

[56] T. Li, Y. Luo, and N. Wang, Compilation of recent nuclear ground state charge radius measurements and tests for models, Atomic Data and Nuclear Data Tables **140**, 101440 (2021).

[57] N. Wang, M. Liu, and X. Wu, Modification of nuclear mass formula by considering isospin effects, Phys. Rev. C **81**, 044322 (2010).

[58] T. Wakasa, M. Takechi, S. Tagami, and M. Yahiro, Matter radii and skins of 6,8he from reaction cross section of proton+6,8he scattering based on the love–franey t-matrix model, Results in Physics **35**, 105329 (2022).